

Composition and formation age of amorphous silica coating glacially polished surfaces

Terrence Blackburn¹, Shalev Siman-Tov², Matthew A. Coble³, Greg M. Stock⁴, Emily E. Brodsky¹, and Bernard Hallet⁵

¹Earth and Planetary Sciences, University of California, Santa Cruz, California 95064, USA

²Geological Survey of Israel, 9371234 Jerusalem, Israel

³Department of Geological Sciences, Stanford University, Stanford, California 94305, USA

⁴National Park Service, Yosemite National Park, El Portal, California 95318, USA

⁵Quaternary Research Center and Department of Earth and Space Sciences, University of Washington, Seattle, Washington 98195, USA

ABSTRACT

Recent micrographs of smooth, glacially abraded silicic bedrock reveal an amorphous coating layer adhering to the bedrock, with structures that tie its formation to glacial abrasion. What remains unclear is whether this coating is formed by the physical comminution of bedrock, resulting in amorphous material with a bedrock composition, or by chemical dissolution of silicate minerals followed by precipitation of an amorphous layer enriched in silica and depleted in cations relative to the bedrock. Here, we report the composition and formation age of the amorphous coatings in Yosemite National Park, California, USA. The coatings are depleted in base cations (50%–90%) and enriched in silica (10%–50%) as well as trace Fe and U (4- to 100-fold) relative to the bedrock, reflecting dissolution by and precipitation from subglacial waters. The ²³⁴U/²³⁸U activity ratio of the amorphous layer is 200%–600% above secular equilibrium, reflecting a surficial U source enriched by α -recoil processes and consistent with the ²³⁴U enrichment observed in subglacial waters. The ²³⁰Th/²³⁸U activity ratio is 30%–100% below secular equilibrium and records Th-U fractionation in subglacial waters at 30–10 ka, consistent with coating formation during the Last Glacial Maximum (LGM). These amorphous coatings are subglacial precipitates that record the chemical weathering of silicates beneath glaciers during the LGM. Collectively, these observations link silicate dissolution and amorphous silica production to physical processes at the glacier bed, a result that may have significant implications for the global Si and CO₂ budgets on glacial-interglacial time scales.

INTRODUCTION

Glaciers are renowned for their ability to physically erode landscapes. This physical erosion occurs beneath glacial ice through sliding at the base of warm-based glaciers by both quarrying and abrasion of bedrock, which produce large volumes of glacial silt- and clay-sized particles. Particle comminution greatly increases the surface area of minerals on which chemical weathering can operate, a process that has been inferred to increase chemical denudation rates above average rates for nonglaciated catchments (Anderson et al., 1997). The composition of subglacial water is distinct from that of nonglaciated catchments and reflects a unique chemical weathering regime beneath glaciers (Anderson et al., 1997; Torres et al., 2017).

The ways in which glaciers chemically interact with the continental crust globally, and the types of weathering reactions that occur are fundamental factors in understanding whether

glaciers operate as a net CO₂ source or sink. This balance ultimately determines the feedbacks between glacial processes and Earth's climate over interglacial-glacial cycles. In studies of modern alpine glaciers, the most abundant solutes in glacial runoff, Ca²⁺, HCO₃⁻, and SO₄²⁻ (e.g., Sharp et al., 1995; Torres et al., 2017), have led to the interpretation that the primary chemical weathering reaction beneath glaciers is the dissolution of carbonates and oxidation of sulfides, a result that holds even though calcite and pyrite are found only in trace abundances in granitic or gneissic catchments (Erel et al., 2004). If the extent of chemical weathering beneath glaciers is indeed limited to reactions with trace carbonate and sulfate, phases that release CO₂ upon dissolving, glaciers are a source of CO₂ and potentially buffer the net cooling that occurs during glacial intervals (Sharp et al., 1995; Torres et al., 2017). Reactions such as the dissolution of silicates would have the opposite effect, releasing both Si and

alkaline metals, with the former drawing down CO₂ during diatom blooms on shorter time scales, whereas the latter may contribute to carbonate formation and CO₂ sequestration on longer time scales (Graly et al., 2017). However, the degree to which silicate weathering occurs beneath glaciers has previously been regarded as highly limited, based on low dissolved Si concentration in glacial runoff (Anderson et al., 1997; Torres et al., 2017).

Emerging data suggest that these observations collected from modern alpine glaciers may not apply to all subglacial settings. Beneath Greenland ice masses, for example, glacial waters can indeed carry significant loads of Si to global oceans, in the form of undissolved amorphous Si grains suspended within turbid glacial runoff, which dissolve upon reaching the saline ocean (Hawkings et al., 2017). Though there is at present no known connection between the formation of these amorphous grains and any specific glacial process, this observation hints that any chemical interaction between glaciers and the siliceous continental crust may be underestimated by a factor of 10 (Hawkings et al., 2017; Torres et al., 2017).

One place to examine the chemical interaction between glacial ice and silicate crust is where rocky outcrops have been eroded and polished by glacial action to a smooth, glossy bedrock surface known as glacial polish. It has been commonly assumed that these mirror-like surfaces are generated by the mechanical process of abrasion during which basal debris-rich ice and rock remove protrusions until a surface is optically smooth (Iverson, 1991). A recent investigation by Siman-Tov et al. (2017) of glaciated crystalline rocks, however, identified an ~1–4- μ m-thick layer of predominantly amorphous material supporting submicron-size mineral fragments that collectively coated the abraded bedrock. This coating was interpreted to record polish formation by a combination of abrasion, removal, and

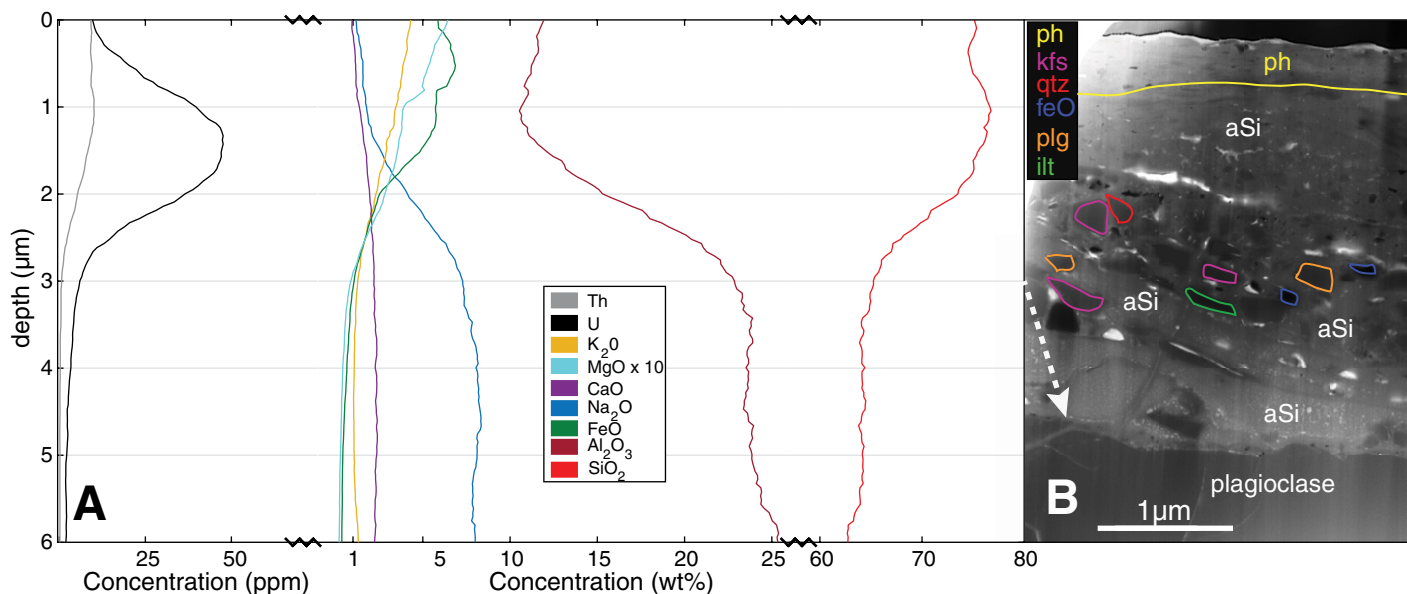


Figure 1. A: Representative laser ablation–inductively coupled plasma–mass spectrometry (LA-ICP-MS) element profile for Daff Dome, Tuolumne Meadows, Yosemite National Park, (California, USA). Note the break in scale after 50 ppm and 25 wt%. See Appendix DR 4 (see text footnote 1) for depth calibration. Gradual chemical transitions are artifacts of mixing between suspended mineral fragments and variations in polish thickness, which can vary by 1–2 μm on horizontal scales (less than 25 μm spot size). **B:** Transmission electron microscope image from Daff Dome reveals mostly amorphous silica (aSi) supporting fragments of quartz (qtz), Fe-oxide (FeO), illite (ilt), and alkali (kfs) and plagioclase (plg) feldspars above host plagioclase and capped by layer of phyllosilicates (ph). Note differing vertical scales for A and B, connected at 3 μm by white dashed arrow.

adhesion of mechanically abraded host rock, ground to submicron-size mineral fragments, and noncrystalline amorphous material that spread over the overlying host rock. Though mechanical processes alone could reduce grain size, yielding amorphous material, as observed in experimental granite gouge (Yund et al., 1990), the amorphous coatings on silicate rock can also occur as a result of chemical weathering, specifically, the dissolution of silicates and reprecipitation amorphous silica. In experimental studies, nanometer-thick layers (<0.1 μm) of hydrated silica form upon exposure of silicates to fluids (Hellmann et al., 2012). These layers are chemically distinct, with high total silica and low base cations relative to the underlying host mineral. If the amorphous material occurring on glacially polished surfaces exhibits similar compositional traits, it suggests (1) a significant role of chemical weathering in polish formation; (2) a likely mechanism for the formation of amorphous silica particles in glacial runoff, which are also found to be enriched in Si and depleted in cations (Hawkings et al., 2017); and (3) a previously unrecognized archive of former glacier sliding and silicate chemical weathering occurring beneath glaciers that has implications for the global Si and CO_2 budgets.

METHODS AND RESULTS

Here, we present the results of a geochemical and isotopic investigation that utilized *in situ* analytical techniques (laser ablation–inductively coupled plasma–mass spectrometry [LA-ICP-MS] and sensitive high-resolution ion microprobe reverse geometry [SHRIMP-RG]) to determine the major, trace, and U-series isotopic composition

of the microns-thick amorphous layer within glacially polished surfaces collected from Yosemite National Park, California, USA (Appendix DR1 in the GSA Data Repository¹). Samples were collected from Lyell Canyon and Tuolumne Meadows, areas dominated by crystalline granodiorite that deglaciated at ca. 15–10 ka (Dühnforth et al., 2010) at the end of the Last Glacial Maximum. In a prior study, these samples were the focus of a microstructural investigation using transmission electron microscopy (TEM) imaging (Siman-Tov et al., 2017) that provide a visual reference for the new geochemical data presented herein.

Composition of the Glacial Polish Layer

The composition of the glacial polish layer was determined using the LA-ICP-MS system at the University of California, Santa Cruz, USA (see Appendix DR2 for methods). A single laser-spot analysis collected from Daff Dome (Daff01) in Tuolumne Meadows provides a representative example of a continuous major- and trace-elemental profile from the polish surface down into the underlying bedrock. In the example shown in Figure 1A, the mineral grain beneath the polish is plagioclase feldspar with high Si, Al, Na, and Ca, but also with detectable K, Fe, and Mg. U and Th concentrations are <5 ppm. Approximately 3 μm below the coating surface, the abundances of all measured elements change. The total silica increases toward the surface, while concentrations

of base cations abundant in the underlying mineral (Na, Ca) decrease. Cations not abundant in host plagioclase (K, Mg, Fe, U, Th) are found at higher concentrations near the surface. Comparison to TEM images from a nearby plagioclase grain (Fig. 1B) revealed a plagioclase capped by an ~3- μm -thick layer of predominantly amorphous material supporting loosely aligned, submicron-size fragments of mostly quartz, plagioclase, and alkali feldspars, as well as Fe oxides.

Multiple laser spot analyses collected from a centimeter-sized glacial polish sample from Daff Dome (Daff01) reveal compositional changes above each rock-forming mineral within the bedrock. A comparison of cation to SiO_2 concentrations for all spot analyses, color coded by ablation depth, permits identification of: (1) the composition of the underlying bedrock minerals (Fig. 2, yellow) and (2) the composition of the polish layer (Fig. 2, green and blue). Na_2O at >3 μm depth (Fig. 2A, yellow), for example, reveals bedrock minerals beneath the polish layer of both Na-enriched and Na-depleted feldspars (~65% SiO_2) along with quartz (~100% SiO_2). At shallow depths (Fig. 2, blue) the composition is relatively uniform (~70–80 wt% SiO_2 , ~1 wt% Na_2O) for the polish layer, independent of the underlying mineral. This observation extends to all measured major elements, suggesting that the polish occupies a relatively narrow compositional space that is distinct from all of the underlying minerals (Figs. 2A–2F).

To determine the chemical processes that are operating to generate the glacial polish layer, we used a cluster analysis to define the polish composition for each laser-ablation spot and compared it to the bulk composition of the underlying host

¹GSA Data Repository item 2019119, sample location and compositional data, as well as laboratory methodologies, is available online at <http://www.geosociety.org/datarepository/2019/>, or on request from editing@geosociety.org.

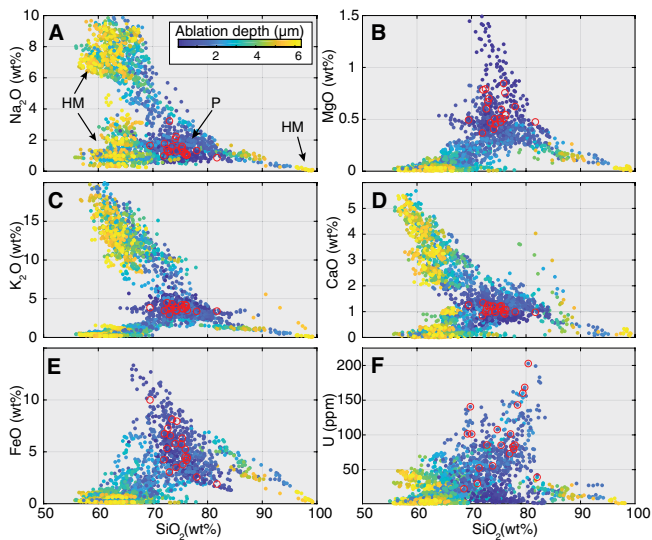


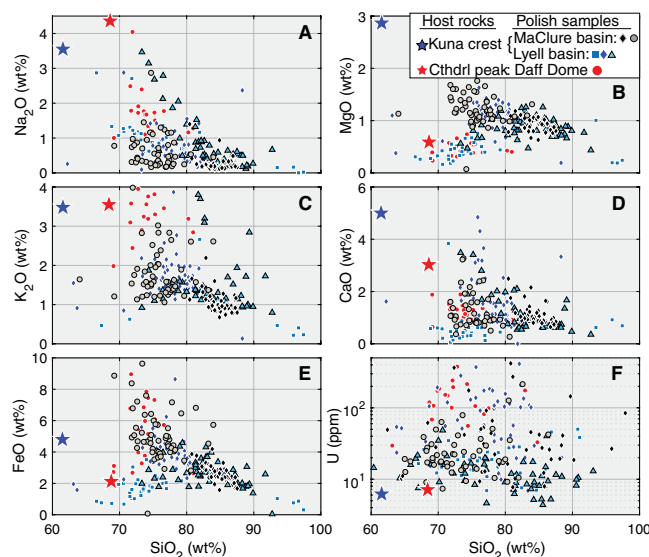
Figure 2. Harker diagrams displaying multiple laser spot analyses from Daff Dome Tuolumne Meadows, Yosemite National Park, (California, USA) colored by ablation depth. HM—underlying host mineral; P—polish. Red open circles are averaged polish compositions for major elements (A–E) and maximum concentration for uranium (F) identified for each laser spot. Polish compositions (open red circles) are compared to whole-rock data in Figure 3.

rock. Polish compositions for each laser spot are shown as red circles for Daff Dome (Fig. 2) and five additional samples from Lyell Canyon (see Appendix DR2). Comparison between polish and bedrock compositions revealed compositional trends that include the enrichment in Si by up to 30 wt% relative to the whole-rock values (Fig. 3). This Si enrichment is coupled with loss of 50%–90% of Na, K, Mg, and Ca relative to bulk bedrock compositions (Figs. 3A–3D). In contrast, U can be enriched in some locations up to 100-fold relative to the bedrock (Fig. 3F).

Subglacial Processes and the Formation Age of the Glacial Polish Layer

U-series decay chain members such as ^{234}U and ^{230}Th can, by chemical or physical processes, be enriched or depleted relative to parent ^{238}U . Fractionation of these “intermediate daughters” can be utilized to measure geologic time and/or reflect the formation environment.

Figure 3. Glacial polish composition for Daff Dome Tuolumne Meadows, Yosemite National Park, (California, USA) (red circles in Fig. 2) and five samples within Lyell Canyon, Yosemite (Appendix DR2 [see text footnote 1]). In comparison to whole-rock values (stars), polish compositions reflect Si (10%–50%) enrichment and cation loss (50%–90%). Whole-rock values are from Bateman et al. (1988) and Gray et al. (2008). Note that Daff Dome polish (red circles) should be compared to Cathedral Peak Granodiorite (red star), while all Lyell Canyon polish formed upon the Kuna Crest Granodiorite (blue star).



U-series (^{230}Th – ^{232}Th – ^{234}U – ^{238}U) determinations of the glacially polished surface from Daff Dome (Daff01) were collected using the SHRIMP-RG ion microprobe. See Appendix DR3 for methods and data table. Multiple spot analyses all occupy a distinct isotopic space where $^{234}\text{U}/^{238}\text{U}$ activity ratios are 200%–600% above secular equilibrium, whereas the $^{230}\text{Th}/^{238}\text{U}$ activity ratios are 30%–100% below. These isotopic compositions can be bracketed by isochronous curves that place ^{230}Th fractionation from ^{234}U over a range of time scales from ca. 30 to 10 ka (Fig. 4).

DISCUSSION

Formation of the Amorphous Layer

Compositional comparison of the polish layer and underlying bedrock suggests that the amorphous layer is not directly related to the underlying bedrock (Fig. 1). Rather, the amorphous layer occupies a relatively narrow

compositional space, distinct from all underlying minerals (Fig. 2), with compositional variability likely attributed to mineral fragments within the layer (e.g., Fig. 1B). Next, the loss of nearly all cations coupled with an increase in SiO_2 (Fig. 3) corresponding to depths imaged as structurally amorphous (Fig. 1B) is consistent with silicate dissolution at the fluid-rock interface followed by the precipitation of amorphous silica from subglacial water (Hallet, 1975; Hellmann et al., 2012; Rutledge et al., 2018).

The role of subglacial fluids is further supported by the high concentrations of U in the polish relative to the bedrock, an observation that requires sourcing outside of the bedrock. This hypothesis is supported by the high $^{234}\text{U}/^{238}\text{U}$ ratios in the amorphous layer (Fig. 4), an observation that indicates a surficial, non-bedrock U source where ^{234}U is enriched by physical fractionation from ^{238}U . The high-energy α -decay of parent ^{238}U housed within silicates results in the ejection of ^{234}U from fine-grained sediments into subglacial fluids or ice. Elevated $^{234}\text{U}/^{238}\text{U}$ values have been observed in glacial runoff (Arendt et al., 2018; Pogge von Strandmann et al., 2006), as well as in subglacial carbonate precipitates (Refsnider et al., 2012), and reflect interaction between rock and ice. A subglacial water source is also supported by the ^{230}Th –U data, which suggest that insoluble ^{230}Th was absent from subglacial waters relative to fluid-mobile U. The isotopic space defined by the amorphous layer records chemical fractionation in subglacial fluids occurring over 30–10 ka, consistent with the formation of amorphous material over a time range spanning the Last Glacial Maximum (Clark et al., 2009) to deglaciation in Yosemite (Dühnforth et al., 2010).

Collectively, we interpret the compositional and isotopic data presented here to record the subglacial dissolution of silicate rock and production of amorphous silica during the LGM. We propose that glacial action comminutes particles at the ice-rock interface, increasing the surface area of silicate wear particles. Glacial sliding is one possible driver for chemical activity at the glacier bed; local pressure melting in high-pressure areas produces undersaturated subglacial waters, which can dissolve minerals, while local freezing in low-pressure areas can consume subglacial water, concentrating solutes to the point of precipitation (Hallet, 1975). Base cations (Na, K, Mg, Ca) largely remain within subglacial waters, while amorphous Si is precipitated, incorporating Fe, U, and the U-series composition of subglacial waters.

Potential Implications for Global Element Cycles

The compositional data and direct images from the glacial polish layer produced at the ice-rock interface suggest a likely location for the generation of amorphous silica grains and coatings to particles observed within glacial runoff (Hawkins et al., 2017). Such a mechanism is

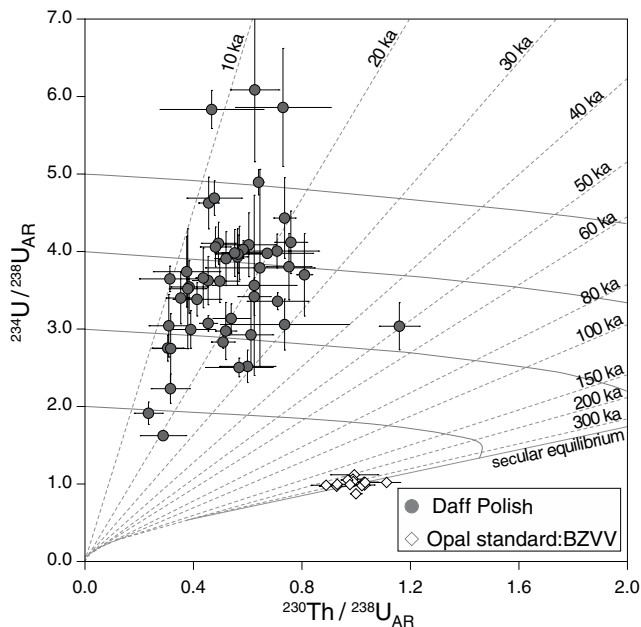


Figure 4. ^{230}Th - ^{234}U - ^{238}U data reported as Activity Ratios (AR) for multiple spots (1σ) measured by sensitive high-resolution ion microprobe–reverse geometry (SHRIMP-RG) on U-rich polish from Daff Dome Tuolumne Meadows, Yosemite National Park, (California, USA). Standard BZVV (Virgin Valley, Nevada, USA) is included. Precipitates forming in absence of ^{230}Th , with a range of $^{234}\text{U}/^{238}\text{U}$ initial values (e.g., system starts along y-axis), evolve to right side as a result of ^{230}Th ingrowth, following blue curves toward secular equilibrium (solid line).

of special interest because enhanced Si delivery to the oceans during glacial intervals could produce diatom blooms, previously hypothesized to account for decreased atmospheric CO_2 during glacial periods (Harrison, 2000), which is consistent with both low Ge/Si values in marine opals (Froelich et al., 1992) and higher Si concentrations in marine sponges (Jochum et al., 2017) formed during glacial intervals. Finally, the data presented here show that the generation of amorphous silica must include the delivery of alkaline metals (e.g., Ca^{2+} , Mg^{2+}) to global oceans, a reaction that could sequester CO_2 on longer time scales should these contributions outweigh subaerial ones.

CONCLUSIONS

We interpret the compositional and isotopic data presented here to record the subglacial dissolution of silicate rock and production of amorphous silica beneath glaciers in the Sierra Nevada, California, during the Last Glacial Maximum. Glacial polish, a ubiquitous feature of glaciated landscapes, is now recognized as being constructed of subglacial chemical precipitates that archive the composition of subglacial waters and permit geochronologic constraints to be placed on the timing of temperate ice cover and subglacial chemical weathering of silicates.

ACKNOWLEDGMENTS

We thank Joseph Graly, Kurt Cuffey, and an anonymous reader for their constructive reviews. Thanks also go to Rob Franks for assisting in data collection and to Ken Ferrier and Joel Blum for insightful discussions. This work was supported by a University of California, Santa Cruz, Faculty Research Grant to Blackburn and Brodsky.

REFERENCES CITED

Anderson, S., Drever, J.I., and Humphrey, N.F., 1997, Chemical weathering in glacial environments: *Geology*, v. 25, p. 399–402, [https://doi.org/10.1130/0091-7613\(1997\)025<0399:CWIGE>2.3.CO;2](https://doi.org/10.1130/0091-7613(1997)025<0399:CWIGE>2.3.CO;2).

Arendt, C.A., Aciego, S.M., Sims, K.W.W., Das, S.B., Sheik, C., and Stevenson, E.I., 2018, Influence of glacial meltwater on global seawater $\delta^{234}\text{U}$: *Geochimica et Cosmochimica Acta*, v. 225, p. 102–115, <https://doi.org/10.1016/j.gca.2018.01.007>.

Bateman, P.C., Chappell, B.W., Kistler, R.W., Peck, D.L., and Busacca, A., 1988, Tuolumne Meadows Quadrangle, California: Analytic Data: Washington, D.C., U.S. Government Publishing Office, 43 p.

Clark, P.U., Dyke, A.S., Shakun, J.D., Carlson, A.E., Clark, J., Wohlfarth, B., Mitrovica, J.X., Hostetler, S.W., and McCabe, A.M., 2009, The Last Glacial Maximum: *Science*, v. 325, p. 710–714, <https://doi.org/10.1126/science.1172873>.

Dühnforth, M., Anderson, R.S., Ward, D., and Stock, G.M., 2010, Bedrock fracture control of glacial erosion processes and rates: *Geology*, v. 38, p. 423–426, <https://doi.org/10.1130/G30576.1>.

Erel, Y., Blum, J.D., Roueff, E., and Ganor, J., 2004, Lead and strontium isotopes as monitors of experimental granitoid mineral dissolution: *Geochimica et Cosmochimica Acta*, v. 68, p. 4649–4663, <https://doi.org/10.1016/j.gca.2004.04.022>.

Froelich, P.N., Blanc, V., Mortlock, R.A., Chillrud, S.N., Dunstan, W., Udomkit, A., and Peng, T.H., 1992, River fluxes of dissolved silica to the ocean were higher during glacials: Ge/Si in diatoms, rivers, and oceans: *Paleoceanography and Paleoclimatology*, v. 7, p. 739–767, <https://doi.org/10.1029/92PA02090>.

Graly, J.A., Drever, J.I., and Humphrey, N.F., 2017, Calculating the balance between atmospheric CO_2 drawdown and organic carbon oxidation in subglacial hydrochemical systems: *Global Biogeochemical Cycles*, v. 31, p. 709–727, <https://doi.org/10.1002/2016GB005425>.

Gray, W., Glazner, A.F., Coleman, D.S., and Bartley, J.M., 2008, Long-term geochemical variability of the Late Cretaceous Tuolumne intrusive suite, central Sierra Nevada, California, in Annen, C., and Zellmer, G.F., eds., *Dynamics of Crustal Magma Transfer, Storage and Differentiation*: Geological Society [London] Special Publication 304, p. 183–201, <https://doi.org/10.1144/SP304.10>.

Hallet, B., 1975, Subglacial silica deposits: *Nature*, v. 254, p. 682–683, <https://doi.org/10.1038/254682a0>.

Harrison, K.G., 2000, Role of increased marine silica input on paleo- $p\text{CO}_2$ levels: *Paleoceanography*, v. 15, p. 292–298, <https://doi.org/10.1029/1999PA000427>.

Hawkings, J.R., Wadham, J.L., Benning, L.G., Hendry, K.R., Tranter, M., Tedstone, A., Nienow, P., and Raiswell, R., 2017, Ice sheets as a missing source of silica to the polar oceans: *Nature Communications*, v. 8, p. 14198, <https://doi.org/10.1038/ncomms14198>.

Hellmann, R., Wirth, R., Daval, D., Barnes, J.-P., Penisson, J.-M., Tisserand, D., Epicier, T., Florin, B., and Hervig, R.L., 2012, Unifying natural and laboratory chemical weathering with interfacial dissolution-precipitation: A study based on the nanometer-scale chemistry of fluid-silicate interfaces: *Chemical Geology*, v. 294, p. 203–216, <https://doi.org/10.1016/j.chemgeo.2011.12.002>.

Iverson, N.R., 1991, Morphology of glacial striae: Implications for abrasion of glacier beds and fault surfaces: *Geological Society of America Bulletin*, v. 103, p. 1308–1316, [https://doi.org/10.1130/0016-7606\(1991\)103<1308:MOGSIF>2.3.CO;2](https://doi.org/10.1130/0016-7606(1991)103<1308:MOGSIF>2.3.CO;2).

Jochum, K.P., Schuessler, J.A., Wang, X.H., Stoll, B., Weis, U., Müller, W.E.G., Haug, G.H., Andreae, M.O., and Froelich, P.N., 2017, Whole-ocean changes in silica and Ge/Si ratios during the Last Deglacial deduced from long-lived giant glass sponges: *Geophysical Research Letters*, v. 44, no. 22, p. 11,555–11,564, <https://doi.org/10.1002/2017GL073897>.

Pogge von Strandmann, P.A.E., Burton, K.W., James, R.H., van Calsteren, P., Gíslason, S.R., and Mokadem, F., 2006, Riverine behaviour of uranium and lithium isotopes in an actively glaciated basaltic terrain: *Earth and Planetary Science Letters*, v. 251, p. 134–147, <https://doi.org/10.1016/j.epsl.2006.09.001>.

Refsnider, K.A., Miller, G.H., Hillaire-Marcel, C., Fogel, M.L., Ghaleb, B., and Bowden, R., 2012, Subglacial carbonates constrain basal conditions and oxygen isotopic composition of the Laurentide Ice Sheet over Arctic Canada: *Geology*, v. 40, p. 135–138, <https://doi.org/10.1130/G32335.1>.

Rutledge, A.M., Horgan, B.H.N., Havig, J.R., Rampe, E.B., Scudder, N.A., and Hamilton, T.L., 2018, Silica dissolution and precipitation in glaciated volcanic environments and implications for Mars: *Geophysical Research Letters*, v. 45, p. 7371–7381, <https://doi.org/10.1029/2018GL078105>.

Sharp, M., Tranter, M., Brown, G.H., and Skidmore, M., 1995, Rates of chemical denudation and CO_2 drawdown in a glacier-covered alpine catchment: *Geology*, v. 23, p. 61–64, [https://doi.org/10.1130/0091-7613\(1995\)023<0061:ROCDAC>2.3.CO;2](https://doi.org/10.1130/0091-7613(1995)023<0061:ROCDAC>2.3.CO;2).

Siman-Tov, S., Stock, G.M., Brodsky, E.E., and White, J.C., 2017, The coating layer of glacial polish: *Geology*, v. 45, p. 987–990, <https://doi.org/10.1130/G39281.1>.

Torres, M.A., Moosdorf, N., Hartmann, J., Adkins, J.F., and West, A.J., 2017, Glacial weathering, sulfide oxidation, and global carbon cycle feedbacks: *Proceedings of the National Academy of Sciences of the United States of America*, v. 114, p. 8716–8721, <https://doi.org/10.1073/pnas.1702953114>.

Yund, R.A., Blanpied, M.L., Tullis, T.E., and Weeks, J.D., 1990, Amorphous material in high strain experimental fault gouges: *Journal of Geophysical Research—Solid Earth*, v. 95, p. 15,589–15,602, <https://doi.org/10.1029/JB095iB10p15589>.

Printed in USA